Korean J Thorac Cardiovasc Surg 2019;52:205-220 □ COLLECTIVE OF CURRENT REVIEW, LECTURE □
ISSN: 2233-601X (Print) ISSN: 2093-6516 (Online) https://doi.org/10.5090/kjtcs.2019.52.4.205

Real-Time Fluorescence Imaging in Thoracic Surgery

Priyanka Das[1,*], Sheena Santos[1,*], G. Kate Park, Ph.D.[1], Hoseok I, M.D., Ph.D.[2,3], Hak Soo Choi, Ph.D.[1]

[1]Gordon Center for Medical Imaging, Department of Radiology, Massachusetts General Hospital and Harvard Medical School, Boston, MA, USA; [2]Department of Thoracic and Cardiovascular Surgery, Pusan National University Hospital, Pusan National University School of Medicine; [3]Biomedical Research Institute, Pusan National University Hospital, Busan, Korea

Near-infrared (NIR) fluorescence imaging provides a safe and cost-efficient method for immediate data acquisition and visualization of tissues, with technical advantages including minimal autofluorescence, reduced photon absorption, and low scattering in tissue. In this review, we introduce recent advances in NIR fluorescence imaging systems for thoracic surgery that improve the identification of vital tissues and facilitate the resection of tumorous tissues. When coupled with appropriate NIR fluorophores, NIR fluorescence imaging may transform current intraoperative thoracic surgery methods by enhancing the precision of surgical procedures and augmenting postoperative outcomes through improvements in diagnostic accuracy and reductions in the remission rate.

Key words: 1. Intraoperative imaging
2. Fluorescence
3. Near-infrared
4. Thoracic surgery
5. Lymph nodes

Introduction

Since the thorax encompasses vital organs such as the heart and lungs, thoracic surgery is not only challenging, but has also become increasingly prevalent in the field of oncology. The evolution of medical imaging modalities has enhanced the diagnosis and treatment of diseases associated with the esophagus, chest wall, and mediastinum, in addition to major organs [1]. Real-time medical imaging enables the holistic observation of the thoracic cavity by utilizing scanning probes and contrast agents to distinguish areas of interest intraoperatively [2]. The implementation of this technology entails the instantaneous acquisition and translation of visual information, transcending the limitations of its predecessors.

Current imaging modalities vary in efficacy for preoperative and operative thoracic procedures. Computed tomography (CT) is a volumetric method that yields 2-dimensional (2D) or 3-dimensional (3D) cross-sectional images with enhanced contrast for soft tissue and image resolution [3]. As nuclear imaging sys-

*These two authors contributed equally to this work.

Received: November 27, 2018, Revised: December 24, 2018, Accepted: December 24, 2018, Published online: August 5, 2019

Corresponding author: Hoseok I, Department of Thoracic and Cardiovascular Surgery, Pusan National University Hospital, Pusan National University School of Medicine, 179 Gudeok-ro, Seo-gu, Busan 49241, Korea
(Tel) 82-51-240-7096 (Fax) 82-51-240-9389 (E-mail) ihoseok@pusan.ac.kr

Corresponding author: Hak Soo Choi, Gordon Center for Medical Imaging, Department of Radiology, Massachusetts General Hospital and Harvard Medical School, 149, 13th Street, Rm 5420, Boston, MA 02129, USA
(Tel) 1-617-726-5784 (Fax) 1-617-643-2604 (E-mail) hchoi12@mgh.harvard.edu

tems, single-photon emission computed tomography (SPECT) and positron emission tomography (PET) can be used to determine the spatial distribution of radiopharmaceuticals in the body and to examine metabolic processes in 3D [4]. Magnetic resonance imaging (MRI) provides high diagnostic value and a strong soft-tissue contrast superior to other imaging modalities, and can be used to monitor physiological processes such as water diffusion and blood oxygenation [5]. Despite these advantages, post-processing, delayed data acquisition, and high costs contribute to the inconvenience of these modalities for intraoperative imaging [6].

In contrast, real-time imaging provides immediate data acquisition, increasing the accuracy and precision of surgical procedures, as well as improving postoperative outcomes and diagnoses. Fluoroscopy projects the movement of contrast agents throughout the body onto a monitor by means of continuous, real-time X-ray imaging [7]. Similarly, ultrasonography provides the immediate acquisition of high-quality images available in both 2D and 3D forms [8]. Although X-ray fluoroscopy and ultrasonography are valuable forms of real-time imaging, exposure to radiation and direct skin contact, respectively, make those modalities unfavorable for invasive thoracic procedures. Surpassing the limitations of those imaging modalities, fluorescence imaging offers safe, cost-efficient, and real-time intraoperative visualization of anatomical structures highlighted by fluorophores [9].

Fluorescence imaging involve 2 fundamental components: fluorophores targeting specific tissues and a fluorescence-detecting imaging system [10]. Ideal fluorophores are highly water-soluble to prevent self-aggregation, are sufficiently photostable in media with serum, and possess superior photophysical properties [2]. Fluorophores are often conjugated to ligands for specific tissue targeting and synthesized with certain functional groups that emit and absorb light within a certain wavelength range. Light energy from an imaging system is used to activate these fluorophores and detect fluorescence produced *in vivo* [11]. The near-infrared (NIR) range (650–900 nm) is the ideal imaging window due to its low absorption and scattering in neighboring tissues, and its reduced autofluorescence *in vivo*. Unlike other medical imaging modalities, fluorescence imaging shows high sensitivity and spatial resolution, which facilitate the visibility of contrast agents even at low concentrations [9]. Since the wavelengths used for fluorescence illumination and color imaging are distinct, only the target specimen is visualized, while excluding background and autofluorescence; this yields a high signal-to-background ratio (SBR) [9-11]. In this review, we discuss intraoperative fluorescence imaging systems and NIR contrast agents for surgical procedures in the thorax, particularly cartilage, vasculature, nerves, sentinel lymph nodes (SLNs), and tumors.

Intraoperative fluorescence imaging systems

Intraoperative fluorescence imaging systems are necessary for improving a surgeon's ability to visualize otherwise imperceptible anatomical structures [9]. The diversity of anatomical structures across patients complicates identification, but fluorescence imaging systems and specific organ-targeting contrast agents allow surgeons to discern each structure on a case-by-case basis. The ideal intraoperative fluorescence imaging system should have a real-time overlay of white-light and fluorescence images, nanomolecular sensitivity, plausible utility during open surgery, and the ability to simultaneously image multiple fluorophores [12]. Currently, most the U.S. Food and Drug Administration (FDA)-approved surgical imaging systems, such as the Hamamatsu Photodynamic Eye (PDE), Fluoptics Fluobeam 800, and Novadaq SPY, are single-channel fluorescence video and image display systems [10,13]. This is disadvantageous, since surgeons require an overlay of the fluorescent dye on a white-light–guided image to properly identify pathological tissues and nearby anatomical structures. Additionally, PDE only provides screen captures, while the Novadaq SPY solely takes images when the target organ or tissue is exposed [12]. New NIR fluorescence imaging systems were developed to improve upon these limitations of intraoperative fluorescence image–guided surgery. Multiple types of real-time imaging systems navigated by NIR fluorophores exist within the category of fluorescence imaging.

1) Multispectral imaging systems

The Fluorescence-Assisted Resection and Exploration (FLARE) imaging system produces an overlaid image

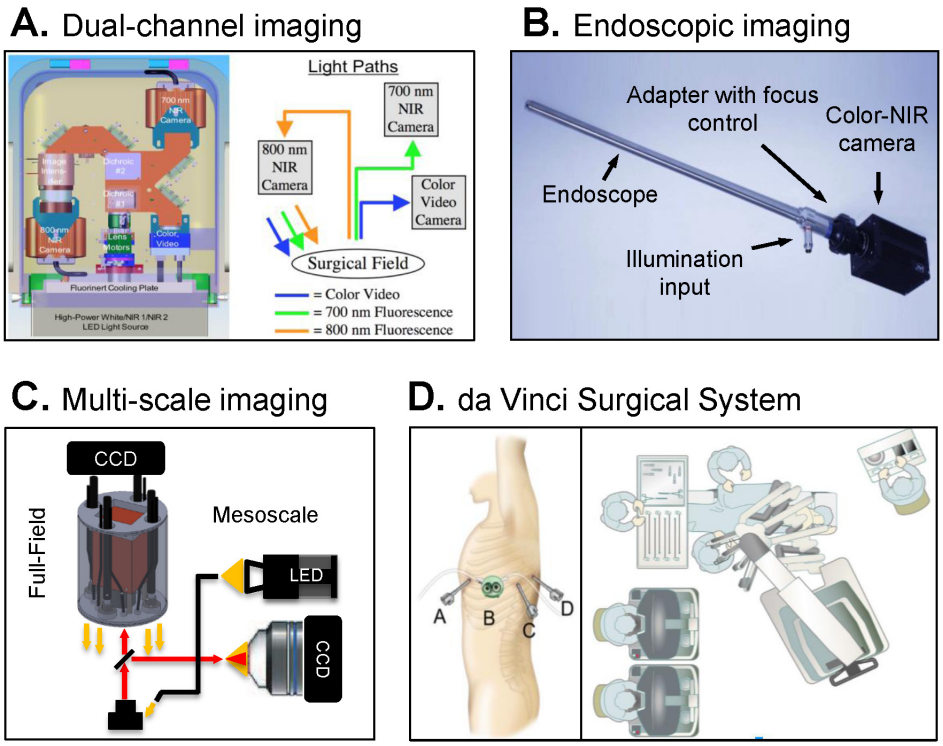

Fig. 1. Intraoperative fluorescence imaging systems. (A) Dual-channel FLARE imaging system [14,15], (B) endoscopic imaging system [19], (C) multiscale multispectral imaging system [10,13], and (D) da Vinci Surgical System [40]. NIR, near-infrared; CCD, charge-coupled device; LED, light emitting diode; FLARE, Fluorescence-Assisted Resection and Exploration.

of invisible NIR fluorescent light and color video, thereby facilitating the identification of clear tumor margins and the avoidance of proximal tissues, nerves, and blood vessels during surgical procedures [10,13]. FLARE consists of 2 separate NIR channels, 2 charge-coupled device cameras (1 for visible light and another for NIR), and dichroic mirrors that are used to focus light onto color video or NIR cameras [14]. The FLARE imaging platform (Fig. 1A) produces real-time color images and videos at wavelengths of 700 and 800 nm [15]. The color video and independent channels continuously acquire fluorescence images at rates up to 15 Hz over a 15-cm-diameter field of view. The fluorescence of organs or tissues in a region is quantified using the custom FLARE software [16]. Different versions of FLARE systems, such as the miniFLARE (Fig. 1B) and K-FLARE (Fig. 1C), employ 2 NIR fluorescence channels working simultaneously with color video, allowing dual-channel imaging of various tissues with the appropriate fluorophores [17-32]. This is beneficial for observing and distinguishing nearby vasculature from critical anatomical structures and tumors during thoracic surgery.

2) Minimally invasive imaging systems

Surgical techniques have evolved from open incisions to minimally invasive surgery, which has numerous benefits compared to conventional open surgery, including reduced bleeding, pain, tissue trauma, and scarring, as well as shorter recovery times and hospital stays [15]. Minimally invasive techniques also exhibit higher accuracy, minimize postoperative complications, and improve cosmesis [33].

An interventional endoscopic imaging system employs an endoscope, a monitor, a video system center, and various light sources for minimally invasive procedures such as thoracoscopy and biopsies associated with cancer diagnosis [34]. Video-assisted thoracoscopic surgery (VATS) provides an alternative to thoracotomy and promotes the use of imaging technology to facilitate minimally invasive surgery [35]. In intraoperative NIR imaging during VATS, an endoscopic camera with an insertion tube, internal instrument channels, and light sources (Fig. 1B) is utilized to measure the fluorescence intensities of contrast agents. Despite groundbreaking developments in this field, intraoperative NIR imaging in VATS applications has several disadvantages, such as its limitation to a 2D surgical field on a monitor, lack

of depth perception, and counterintuitive movement using long rigid instruments and ribs as fulcrum points [36]. This lack of maneuverability hinders accessibility and the efficiency of fine dissection, both of which have been improved by robotic assistance.

3) Robot-assisted thoracic surgery

The da Vinci Surgical System has transformed minimally invasive surgery since its approval by the FDA in 2000 [37]. General thoracic surgeons have successfully performed procedures including esophagectomy, thymectomy, cardiomyotomy, lymph node (LN) dissections, pulmonary lobectomy, and mediastinal mass excisions using this robot-assisted thoracic surgery (RATS) technique. Furthermore, the integration of NIR fluorescence imaging within the da Vinci system has proven to be a feasible way to enhance intraoperative RATS. Wagner et al. demonstrated the efficacy of combining a contrast agent with the da Vinci system for obtaining high-resolution NIR images of the contralateral phrenic nerve in real-time thoracic surgery [38].

The robotic system consists of 3 major components (Fig. 1D): a robot/patient complex where endoscopic ports on the robotic arms are inserted in the patient, a console for the operating surgeon, and a vision cart including optical devices for the robotic camera [39]. Instead of directly operating on the patient with surgical tools, highly sensitive motion sensors on the console translate the surgeon's movements to the instruments of the robotic arms. This console also includes the 3D image and fluorescence viewer, the master hand controls, the footswitch panel used to control electrocautery and to switch between the surgical arms, and the endoscopes. The vision cart monitor provides a view of the operative field to the staff while the electrosurgical unit supplies monopolar and bipolar energy to the instruments on the patient cart [40].

Compared to conventional open surgery and VATS techniques, RATS enables highly accurate surgical procedures by providing 3D visualization of the operative field and improved maneuverability [40]. Although many have studies revealed that physicians may not need prior experience with VATS, or laparoscopic and thoracoscopic surgery, to adapt to RATS, surgeons do need to familiarize themselves with how to use this advanced equipment and technique during the learning curve [41]. The combination of NIR fluorescence probes and RATS imaging systems may improve thoracic surgery by minimizing the overall number of resections and incisions.

Near-infrared fluorescent contrast agents for thoracic surgery

NIR fluorophores play an integral role in intraoperative imaging because they emit and absorb light energy in the optical window of 650–900 nm, enabling the absorption of endogenous biomolecules such as water, melanin, proteins, and hemoglobin in the 200–650 nm range [2,11,26]. Tissues express minimal ab-

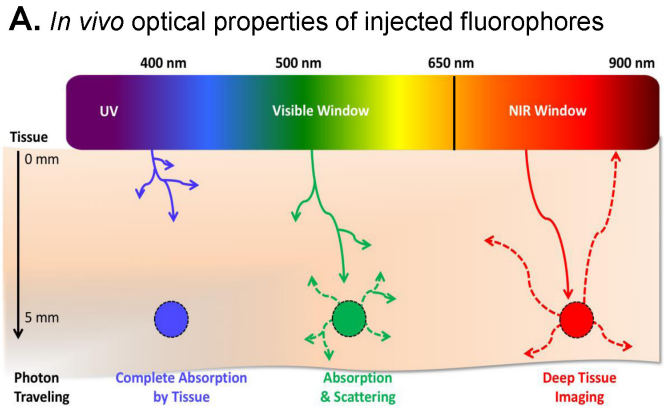

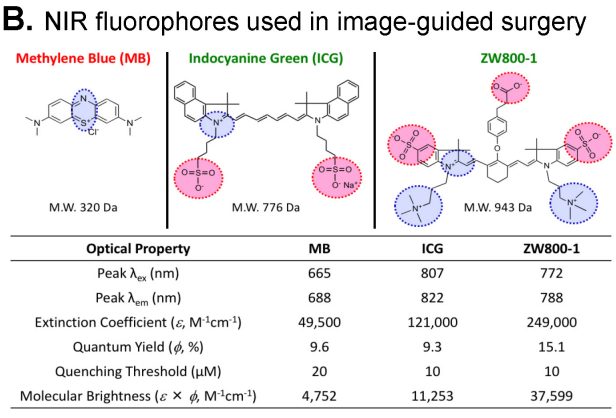

Optical Property	MB	ICG	ZW800-1
Peak λ_{ex} (nm)	665	807	772
Peak λ_{em} (nm)	688	822	788
Extinction Coefficient (ε, $M^{-1}cm^{-1}$)	49,500	121,000	249,000
Quantum Yield (ϕ, %)	9.6	9.3	15.1
Quenching Threshold (μM)	20	10	10
Molecular Brightness ($\varepsilon \times \phi$, $M^{-1}cm^{-1}$)	4,752	11,253	37,599

Fig. 2. The NIR window and NIR fluorophores for image-guided surgery. (A) *In vivo* penetration of fluorescence light and photon travel according to wavelength [9], and (B) chemical structures and optical properties of NIR fluorophores for MB, ICG, and ZW800-1 [15]. NIR, near-infrared; MB, methylene blue; ICG, indocyanine green.

sorbance and fluorescence within this optical window, prompting the development of novel fluorophores in the NIR range (Fig. 2A). Unfortunately, indocyanine green (ICG) and methylene blue (MB) are the only 2 NIR fluorescent small molecules that are currently available in clinics (Fig. 2B).

While ICG has shown great potential for thoracic surgery, there is a clinical need to develop better target-specific NIR fluorophores for intraoperative imaging and image-guided surgery. Since anatomical structures and vasculature are imperceptible under white light, surgeons may easily make mistakes and inflict iatrogenic damage on patients. In the future, surgeons should be able to incorporate multiple NIR fluorophores that target tumors while differentiating nerve tissue from critical blood vessels. Hence, the development of specifically targeted NIR contrast agents is vital for future advancements in thoracic surgery [2,9].

1) Cartilage-targeting contrast agents

Cartilage, albeit difficult to image, is a crucial anatomical structure incorporated within the rib cage, trachea, intervertebral space, and sternum that surgeons must navigate around to avoid serious complications during thoracic surgery [42]. CT scans are inefficient for imaging cartilage due to low X-ray absorption [22], while MRI lacks efficacy because cartilage is an avascular and water-deficient connective tissue. Additionally, there has only been 1 significant study that utilized SPECT radiotracers to target cartilage during the past decade [43]. Unlike these imaging modalities, fluorescence imaging visualizes cartilage-targeting fluorophores instead of the bone itself, generating better real-time images [22]. Fig. 3 exhibits the intraoperative imaging of NIR fluorescent C700-OMe in the costal cartilage of CD-1 mice and Yorkshire pigs [22], along with the bone-specific imaging of P800SO3 [23]. The use of NIR fluorophores is a monumental and noninvasive innovation for determining whether cartilage degeneration has occurred and performing image-guided surgery [44].

2) Vasculature- and nerve-targeting contrast agents

Arterial and peripheral nerve damage often occurs in association with many thoracic surgery procedures, including coronary artery bypass grafts and breast cancer surgery [45]. Due to iatrogenic damage, many patients experience postoperative complications such as loss of function, weakness, muscle atrophy, fasciculation, paralysis, cardiac irregularities, allodynia, and chronic neuropathy [46]. Iatrogenic damage

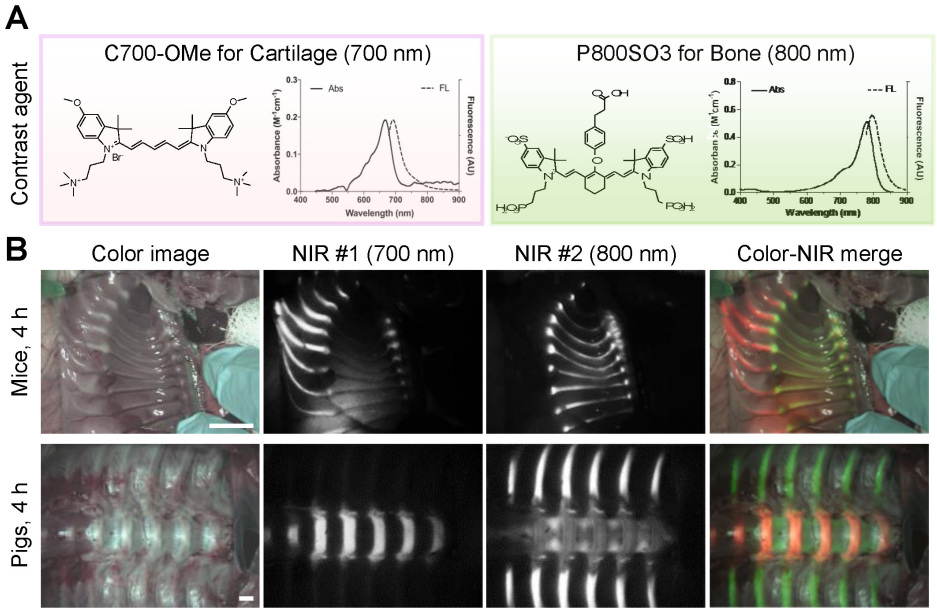

Fig. 3. Dual-channel imaging of cartilage and bone. (A) Chemical structures of C700-OMe [22] and P800SO3 [23] for cartilage- and bone-specific imaging, respectively. (B) Simultaneous cartilage and bone imaging in mice (top) and pigs (bottom). Scale bars=1 cm. C700-SO3 and P800-SO3 were injected intravenously 4 hours prior to imaging [22].

can be attributed to the lack of available imaging technology for identifying nerve tissue and vasculature specific to the patient. Although some new technologies are available for visual identification, such as intraoperative electrical stimulation devices, a surgeon's ability to carefully avoid nearby vasculature and nerves is highly dependent on experience [47]. Even so, identifying nerves by their physical appearance and approximate anatomical location may be inconsistent due to the intricacy and size of individual nerves [48]. The development of new NIR fluorophores and optical imaging systems may satisfy the high demand for nerve and vasculature visualization during intraoperative imaging and image-guided surgery.

Over the past decade, ICG has been the primary NIR contrast agent used to visualize critical nerves and arteries in diseased tissues. As shown in Fig. 4A, ICG was used to distinguish atherosclerotic rabbit arteries from normal rabbit arteries [49]. Another study revealed how ICG fluorescence could clinically detect arterial and vascular blood flow in the esophagus just 1 minute after an intravenous injection, assisting the evaluation of the appropriate microvascular anastomotic sites [50]. Additionally, as shown in Fig. 4B, cardiac vessels could be highlighted through the perfusion of IR786-labeled multipotent progenitor cells in a swine model [51]. Real-time myocardial distribution tracking was possible at 1 hour post-injection, showing evidence of progressive vessel plugging after intracoronary delivery. That study demonstrated the immediate delivery and retention of injected stem cells in the infarcted heart, establishing that NIR imaging may play a critical role in improving current cardiac cell therapies [51]. Although the dye was used to track myocardial distribution, its applications may also be extended to highlight areas affected by cardiovascular diseases, which would be revolutionary for thoracic surgeons.

Aside from targeting vasculature, it is also important to focus on developing NIR nerve-targeting fluorophores. The fluorescent labeling of nerves not only diminishes patient morbidity, including numb-

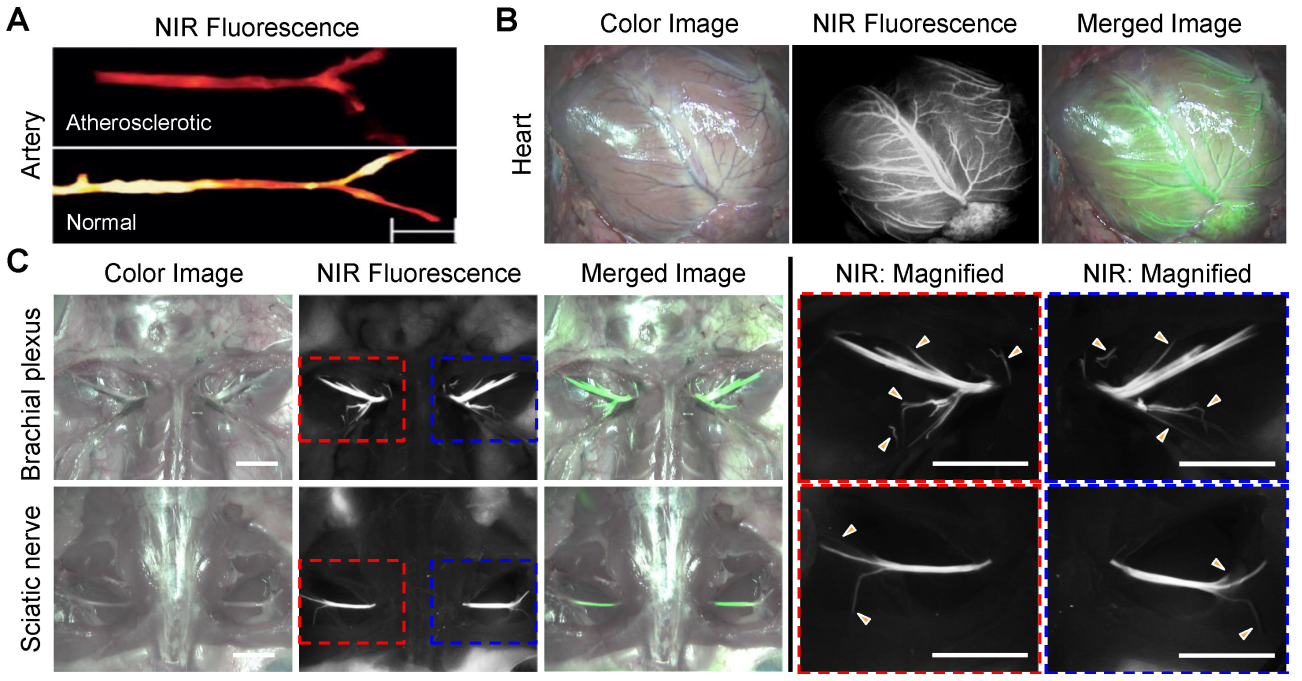

Fig. 4. Intraoperative imaging of vasculature and nerves. (A) Atherosclerotic (top) and normal (bottom) arteries from a rabbit injected with 1.5 mg/kg of ICG 45 minutes prior to imaging [49]. Scale bar=2 cm. (B) Intraoperative cardiac imaging using IR786-labeled bone marrow stem cells in a Yorkshire pig [1]. (C) Intraoperative imaging of brachial plexus and sciatic nerve 4 hours post-injection of Ox4 (200 nmol) in Sprague-Dawley rats [56]. Arrowheads indicate fluorescence signals in nervous tissue and bundles. Scale bars=1 cm. NIR, near-infrared; MB, methylene blue; ICG, indocyanine green.

ness, pain, and localized paralysis, but also improves postoperative outcomes by enhancing the contrast between nerves and adjacent tissues during surgery. The ideal nerve-specific contrast agent for image-guided surgery must reflect the following criteria: (1) a logD at pH 7.4 between 0.5 and 3 and a molecular weight ＜500 Da to maximize blood-nerve-barrier penetration, (2) excitation and emission wavelengths in the NIR window, and (3) prolonged retention in the nerve tissue [52]. ICG has frequently been used to perform intraoperative real-time imaging of thoracic sympathetic nerves, and a previous study highlighted a rabbit's second (T2) to fifth (T5) thoracic ganglia on both sides of the spine under a dual-channel fluorescence imaging system [53]. Gibbs et al. used the visible fluorophores BMB (500 nm) and GE3082 (600 nm) to highlight vessels and the brachial plexus nerve [54]. ICG was used to visualize nearby arteries and vessels, while GE3082 targeted nerve and adipose tissue under the dual-channel FLARE imaging system. However, since both ICG and GE3082 are not very specific to nerves, long-term labeling for guidance cannot be achieved during thoracic surgery, and thus, new nerve-targeting agents must be developed.

Recently, Hingorani et al. [55] prepared the nerve-binding peptide-fluorescein conjugate FAM-NP41 and its human translation (HNP401), which selectively targeted *in vivo* rodent nerves and *ex vivo* human nerves, respectively. Our group synthesized a series of oxazine derivatives and found that oxazine 4 (Ox4) likely binds to the multilayered myelin sheath and interacts with lipids in the myelin membrane [56]. Ox4 exhibits peak emission in the NIR window and clearly visualizes peripheral nerve branches, including the sciatic nerves and the brachial plexus, in mice, rats, and pigs up to 12 hours after an intravenous injection (Fig. 4C). The dosage administered to small and large animals is 10- to 50-fold lower than that of previous dyes, with a human dosage equivalent to 0.25 mg/kg, consistent with the clinically approved dosage of ICG [57]. Despite these major advancements in nerve targeting contrast agents, there is much to be improved upon. For example, currently there are no fluorophores that have been developed to target intercostal nerves, which are very thin and almost indistinguishable to the human eye. Such NIR fluorophores would help surgeons perform thoracic surgery more efficiently.

3) Thymus-targeting contrast agents

Thymic imaging contributes to thoracic surgery by allowing surgeons to familiarize themselves with various types of normal and ectopic locations of thymic tissue. The thymus undergoes many morphological changes in an individual's lifetime and may often be mistakenly interpreted as abnormal without a proper diagnosis [58]. Since the thymus is an integral component of the immune system, serving as the site of T-cell maturation, the repercussions of misdiagnosis can be severe [29]. Currently, conventional medical imaging modalities, including radiography, ultrasonography, CT, MRI, and PET, are used for thymic imaging, but challenges related to safety and sensitivity remain (Fig. 5A). For example, radiography and CT expose patients to radiation, while MRI requires extensive post-processing. Furthermore, although ultrasonography may provide real-time imaging, the shape of the thymus may be affected by cardiac pulsations and respiratory function during procedure, making it difficult to diagnose the thymus (Fig. 5B) [59]. Lastly, for PET imaging of thymic hyperplasia, radiologists may mistake swelling as a sign of recurrent lymphedema, since normal thymic tissue is generally imperceptible (Fig. 5C) [59]. Fluorescent imaging, in contrast, avoids exposing patients to radiation, the complications of post-processing, and unclear imaging. Up until now, no NIR fluorophores have been developed for targeting the thymus. Very recently, Wada et al. [29] successfully targeted thymic tissue after a single intravenous injection of Ox170 in rodents (Fig. 5D) and pigs (Fig. 5E). Ox170 was able to highlight the thymus starting from a dose of 100 nmol in a mouse and 10 μmol in a pig. The results of this study may transform the way thoracic surgeons perform image-guided surgery and attenuate cases of iatrogenic damage in the future.

Intraoperative thoracic tumor diagnosis and surgery

NIR imaging offers a way to reduce the margin of error associated with tumor identification and resection [6,60]. The current thoracic imaging modalities used to diagnose tumors and small nodules in the thoracic region are insufficient and often lead to

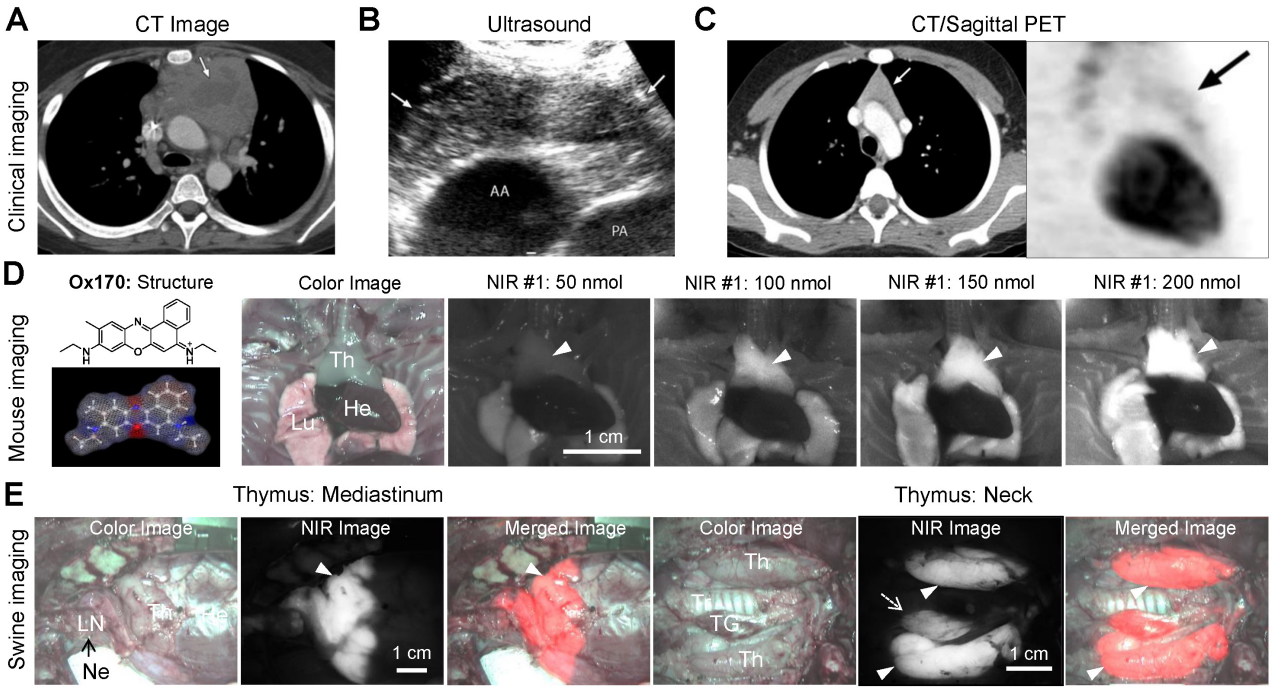

Fig. 5. Clinical imaging of the thymus in young child patients and preclinical imaging of the thymus in rodents and pigs. (A) CT scan shows a thymus with enlarged lymph nodes and a thymic mass with a necrotic core [59]. CT, computed tomography. (B) Ultrasound of a normal thymus (arrows) with smooth borders and echotexture between liver and thyroid [59]. AA, aortic arch; PA, pulmonary artery. (C) A CT/sagittal positron emission tomography scan showing a normal thymus in a young patient with Burkitt lymphoma injected with 18F-FDG [59]. Arrows indicate thymic tissues without FDG avidity. FDG, fludeoxyglucose. (D) Chemical structure of Ox170 and intraoperative thymus imaging in mice. Dose-dependent imaging of Ox170 was obtained 4 hours after an intravenous injection [29]. (E) 10 μmol of Ox170 was injected into 35-kg Yorkshire pigs 8 hours prior to imaging [29]. Th, thymus (arrowhead); He, heart; Lu, lung; LN, lymph node; Ne, nerve; Tr, trachea; TG, thyroid gland (arrow). Scale bars=1 cm.

false positives and false negatives with 18F-fludeoxyglucose-PET scans [61]. In many cases, tumors are undetectable, and if resected improperly, they could regrow and cause remission. Real-time fluorescence imaging would allow surgeons to eradicate all visible tumors, even those smaller than 5 mm.

1) Tumor identification and resection

The development of new NIR tumor-targeted contrast agents is highly anticipated, since they would be able to highlight tumor structures during thoracic surgery and enhance high-precision surgical procedures. By using a combination of NIR fluorophores and an intraoperative real-time imaging system, surgeons would be able to properly identify and obtain margins during the resection of solid tumors. Currently, many preclinical studies are conducting *in vivo* tests to determine the functionality of nonspecific tumor targeting agents. Ofori et al. [62] synthesized a series of NIR fluorescent probes that promote cellular retention during protease activation. These probes demonstrated tumor-specific retention, fast activation kinetics, and fast systemic distribution; furthermore, they were compatible with the FDA-approved da Vinci surgical system for image-guided tumor resection. Fig. 6A shows an image of lung adenocarcinomas in KrasLSL-G12D/+; p53flox/flox; R26LSL-tdTomato/+ mice that had been intravenously injected with the targeted probe 6CQNIR. Intraoperative images were obtained 6 hours post-injection under the da Vinci system. The probe targeted tumors in the lungs, and hematoxylin and eosin staining confirmed the presence of cancerous cells [62]. In a separate study, Predina et al. [63] successfully used ICG to resect thymic carcinosarcomas from a patient who underwent neoadjuvant chemotherapy (Fig. 6B). Complete resection of anterior mediastinal sarcomas is quite challenging due to their proximity to critical struc-

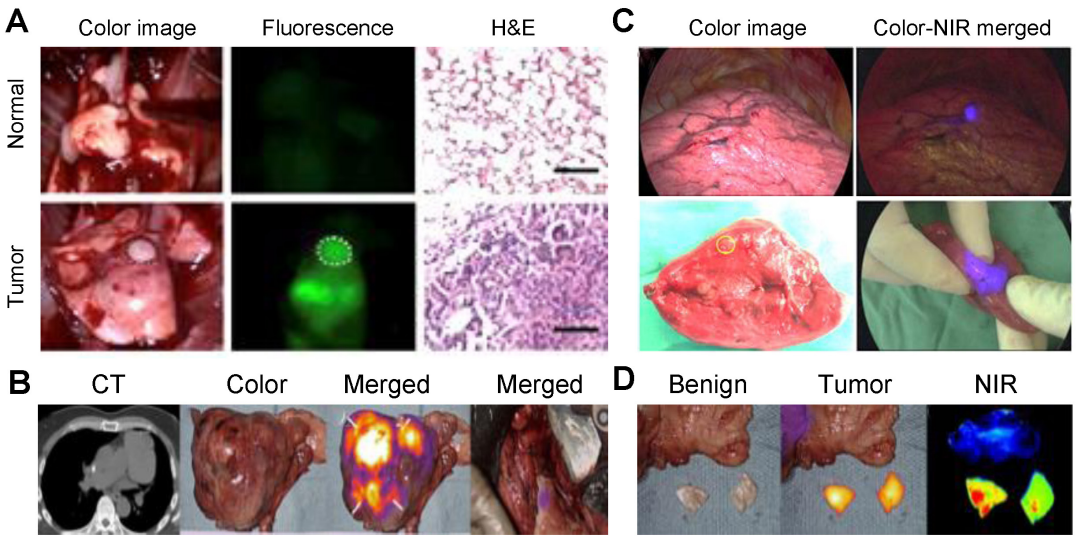

Fig. 6. Intraoperative tumor-specific imaging in lungs. (A) Adenocarcinomas in a lung tumor mouse model injected with 6CQNIR fluorophores (20 nmol) 6 hours prior to imaging [62]. Cancerous lung tissues highlighted with increased fluorescence (white dashed circle) were then analyzed by hematoxylin and eosin (H&E) staining. Scale bars=100 μm. (B) Preoperative CT and intraoperative fluorescence imaging of thymic carcinosarcoma [63]. An anterior mediastinal mass was resected in a patient with primary sarcoma via NIR fluorescence image guidance after injecting ICG 24 hours prior to resection (5 mg/kg). (C) Thoracoscopic tumor imaging highlighted by a percutaneous injection of ICG (0.5 mL; $<$0.125 mg/mL) 15 minutes prior to imaging into lung cancer patients [65]. Lobectomy of primary lung cancer was performed in all patients. Resected tumor specimen with lung nodule highlighted in yellow circle. (D) NIR imaging was used to detect a pulmonary nodule tumor 24 hours after injection of 5 mg/kg of ICG during open thoracotomy [66]. H&E staining was performed on resected tumors and an NIR microscopy image was taken under a 760-nm light source at ×100 magnification. NIR, near-infrared; ICG, indocyanine green; CT, computed tomography.

tures such as the phrenic nerve, heart, and major vessels. Additionally, patients who require mediastinal dissection procedures often undergo neoadjuvant chemotherapy, which makes it difficult for surgeons to identify and determine a margin assessment for tumors. In that study, 5 mg/kg of ICG was administered intravenously 24 hours prior to resection, enabling the identification of the anterior mediastinal tumor mass in the left pulmonary artery [63].

Aside from detecting thymic tumors, NIR imaging is also useful for detecting lung nodules. Typically, the detection of pulmonary nodules is dependent on CT scans and finger palpation, but these methods are unable to thoroughly detect small and soft nodules [64]. Wen et al. [65] revealed that the combination of VATS and NIR fluorescence imaging was effective through the localization and resection of lung nodules in 26 patients who underwent ICG marking with cone-beam CT (Fig. 6C). Another study conducted by Okusanya et al. [66] showed that ICG and NIR imaging enabled the recognition of 5 additional malignant nodules in patients undergoing thoracotomy (Fig. 6D).

Additionally, NIR dyes and a fluorescence imaging system have proven useful for detecting gastrointestinal stromal tumors (GISTs), which are a rare type of sarcoma that predominantly emerge in the stomach and small intestine. GISTs that form outside of the GI tract, namely esophageal GISTs, are rare and therefore poorly diagnosed. The lack of clinicopathological data impedes the identification and surgical resection of GISTs [67]. Although PET, CT, and endoscopy are most commonly used for GIST diagnosis, they are not ideal methods due to high radiation exposure and low GIST specificity [68]. Recently, Kang et al. [69] developed theranostic nanocarriers (a.k.a., "H-Dots") that deliver the anticancer drug imatinib specifically to tumors with rapid renal clearance. H-Dots undergo rapid systemic circulation and whole-body distribution, target tumors efficiently, reduce nonspecific background uptake, and enhance the target-to-background ratio. Experiments with genetically-engineered GIST-bearing mice demonstrated that these NIR fluorescent GIST-targeting nanoprobes, coupled with the appropriate anticancer drugs, may overcome the restrictions and

Table 1. Preclinical sentinel lymph node mapping using near-infrared fluorescence

Organ/tissue	Organism	Fluorophore	HD (nm)	Charge	Reference
Lung	Pig	NIR-QD	15–20	> −100	Soltesz et al. [73] (2005)
Mammary tissue	Mouse, rat, pig	NIR-QD	15–20	> −100	Kim et al. [74] (2004) Frangioni et al. [75] (2007)
Pleural space	Rat, pig	NIR-QD	15–20	> −100	Parungo et al. [77] (2005)
Pleural space	Rat, pig	HSA-78	7.4	−27	Parungo et al. [76] (2004)

HD, hydrodynamic diameter; NIR-QD, near-infrared quantum dot; HSA-78, IRDye78-conjugated human serum albumin.

side effects of conventional imaging modalities and chemotherapies. The clinical translation of these theranostic H-Dots may provide surgeons with specific, sensitive, and real-time image guidance for efficient intraoperative resection [69]. With the help of tumor-targeting NIR dyes and a fluorescence imaging system, surgeons will be able to easily discern tumors that are usually undetectable by the human eye, ultimately optimizing patient care in the long run.

2) Sentinel lymph node mapping

Patients with afflicted LNs have a higher risk of metastasis; thus, early detection and removal of SLNs can decrease this risk [40]. SLNs are the first nodes that receive lymphatic drainage from a tumor, which is why the status of SLNs is the most crucial primary indicator of cancer prognosis. Existing methods of mapping SLNs using MB and radionuclides lack efficacy, as blue dye limits the visualization of lymphatic vessels and SLNs through the skin and fatty tissue, while radioactive tracers require consultation with nuclear specialists [70]. Alternatively, NIR fluorescence imaging provides low tissue autofluorescence, high photon penetration into living tissue, and a high SBR [71]. SLN-targeted fluorophores, combined with NIR intraoperative imaging, are the gateway to image-guided SLN biopsies.

Several preclinical studies have reported the successful use of quantum dots (QDs) and human serum albumin–conjugated fluorophores for SLN mapping of the lung, mammary tissue, and pleural space in mice, rats, and pigs [72-77]. Due to their anionic surface charges and hydrodynamic diameters ranging from 15 to 20 nm, NIR fluorescent QDs are known to be ideal for SLN mapping (Table 1) [73-77]. However, QDs are composed of heavy metals and are potentially toxic for clinical use. To overcome this limitation, Chi et al. [78] conducted a study that demonstrated the potency of ICG for SLN detection in nude mice and breast cancer patients (Fig. 7A–C). ICG is an FDA-approved alternative small molecule (1.2 nm in diameter) with a hydrophobic core and 2 negative charges. Preclinical and clinical studies have not only proven that an increased ICG concentration improves SLN identification and median SBR, but also established that NIR imaging can be used to visualize the migration of ICG from the injection site, through the lymphatic pathway, and into the SLN both *in vivo* and *ex vivo*. Additionally, Ashitate et al. [31] and Wada et al. [32] developed various organic fluorophores for targeting pan LNs in addition to SLN mapping [30]. Particularly, using the independent 700 nm and 800 nm imaging channels, both pan LNs and SLNs were diagnosed simultaneously and separately in rodent and swine models [30,31]. As shown in Fig. 7D, 700 nm ESNF14 (for pan LN mapping) was injected intravenously 4 hours prior to the operation and 800 nm ZW800-3s (for SLN mapping) was injected intradermally 5 minutes prior to imaging [31]. The merged image clearly delineated lymphatic flow in red, pan LNs in lime green, and SLNs in yellow because of the overlapping red and green colors. The dual NIR capabilities of the FLARE imaging system permitted highly-sensitive, real-time, intraoperative identification of all LNs present in the surgical field, as well as definitive identification of the SLN [31]. This can be an excellent tool for simultaneous tumor targeting and SLN mapping in the same subject.

Imaging within the NIR optical window of the ICG fluorescence spectrum facilitates tracing SLNs by enabling the visualization of subcutaneous lymphatic flow [79]. NIR fluorescence imaging systems would utilize ICG in clinical practice to visualize SLNs and lymphatic routes subcutaneously in real time, thereby improving SLN detection and resection in cancer patients. After the lymph drainage pathway is identified, the skin incision site would be marked to locate

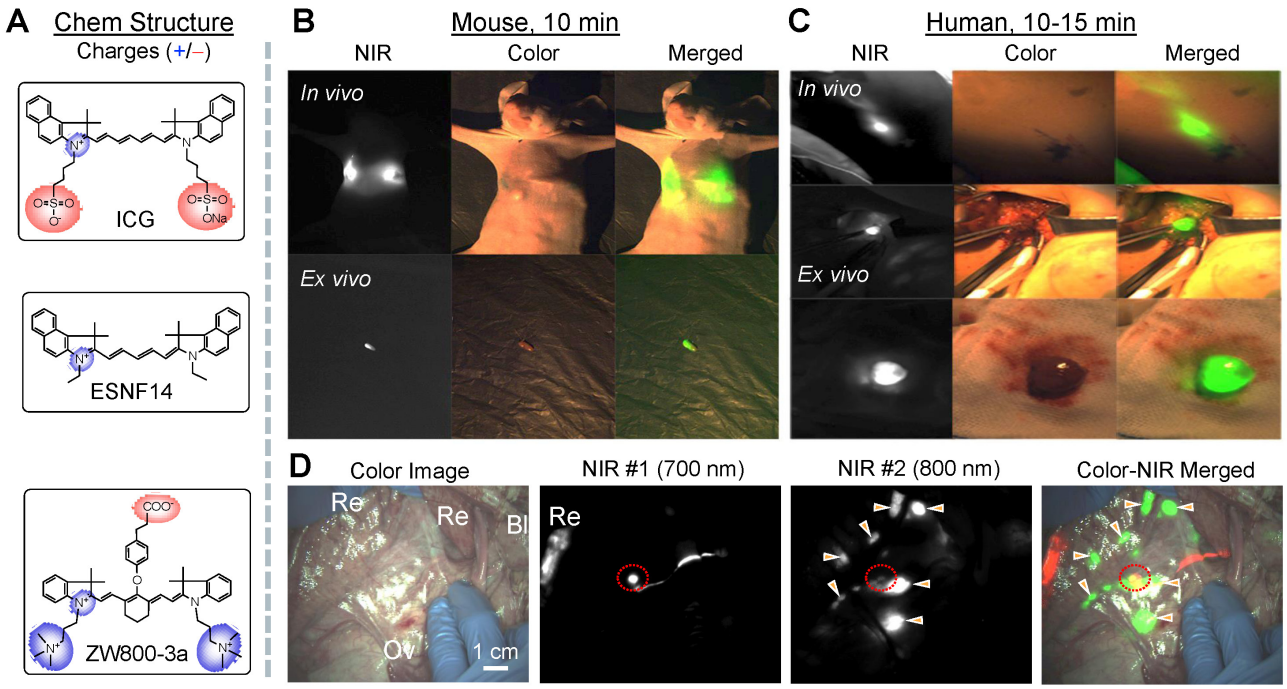

Fig. 7. SLN resection in mice, pigs, and humans using small-molecule fluorophores. (A) Chemical structures of ICG, ESNF14, and ZW800-3a. (B) 100 nmol (0.1 mL, 1 mg/mL) of ICG solution was injected into the armpit of a mouse 10 minutes prior to imaging and resection. NIR, color, and merged images obtained before and after resection of SLNs [78]. (C) NIR fluorescence-guided SLN mapping and resection was performed in humans 10–15 minutes after injection of ICG (1–2 mL, 2.5 mg/mL) [78]. (D) Dual-channel intraoperative NIR imaging of pan lymph nodes and SLN mapping. ESNF14 (5 nmol) was injected intradermally (NIR #1, red) and 320 nmol of ZW800-3a (NIR #2, lime green) was injected intravenously into the same Yorkshire pig 5 minutes and 4 hours before imaging, respectively [31]. Circle indicates SLN; arrowheads indicate pan lymph nodes. SLN, sentinel lymph node; ICG, indocyanine green; NIR, near-infrared.

Table 2. Clinical SLN mapping and resection by near-infrared fluorescence using indocyanine green

Year	No. of patients	Success (%)	No. of SLNs	Reference
2008	25	100	5.4	Tagaya et al. [82] (2008)
2009	6	100	1.5	Troyan et al. [14] (2009)
2010	43	97.7	2.0	Hirche et al. [81] (2010)
2011	50	100	3.7	Tagaya et al. [84] (2011)
2012	24	95.8	1.5	Van der Vorst et al. [85] (2012)
2013	32	100	1.0	Schaafsma et al. [86] (2013)
2013	22	100	2.7	Chi et al. [78] (2013)
2014	96	96.9	3.8	Tong et al. [87] (2014)
2015	168	100	3.0	Toh et al. [88] (2015)
2016	821	97.2	2.3	Sugie et al. [79] (2016)
2017	60	100	2.95	Liu et al. [89] (2017)
2017	200	97	3.0	Guo et al. [83] (2017)
2018	99	98	2.2	Papathemelis et al. [90] (2018)

SLNs, sentinel lymph nodes.

the SLN. SLN biopsies could reduce the extent of radical axillary LN dissection and its subsequent symptoms of morbidity including pain, impaired sensitivity, and lymphedema [80]. Moreover, observing the lymphatic drainage route in real time allows the SLN biopsy to begin once the flow reaches the axilla, reducing the risk of labeling non-SLNs, while yielding high detection rates and low false-negative rates

[81]. Table 2 displays clinical studies conducted over the past 10 years that have demonstrated the efficacy of NIR fluorescence imaging using ICG for SLN detection in breast cancer [14,78,79,81-90]. The results of SLN biopsies exhibited an identification rate of 95.8%–100%, with a mean of 1.0–5.4 SLNs detected per patient.

Conclusion

A myriad of preclinical and clinical studies have demonstrated how different contrast agents, combined with real-time NIR imaging, can enable thoracic surgeons to identify the anatomical structures of vital tissues. Despite its efficacy, some challenges still exist when using fluorescence imaging for thoracic surgery, most notably (1) the lack of quantitative evaluation techniques, (2) the shallow penetration of fluorescent light, and (3) the lack of FDA-approved fluorophores. Further technological advances and investigations are needed to establish techniques for the quantitative measurement and analysis of NIR fluorescence. For example, Yamamoto et al. addressed this drawback and proposed combining ICG imaging and transit time flow measurements in cardiovascular surgery in order to enhance the quantitative assessment of ICG intraoperatively [91]. Additionally, current fluorescence imaging lacks standardization in terms of imaging devices. Creating a consensus document that evaluates each system's performance metrics such as excitation light leakage, field of view, and camera integration times would contribute to standardization [92]. Since the misdiagnosis of tumors can cause great complications, distinguishing false-positive and negative fluorescence findings would be the next development of NIR imaging [93]. Furthermore, although ICG is clinically approved, its composition (containing sodium iodide) can cause allergic reactions in patients [94]. Lastly, the contrast agent can only image superficial processes due to its low tissue penetration [95]. New NIR, and possibly NIR-II, contrast agents should therefore be developed to overcome these limitations. NIR-Ib and NIR-II fluorophores have an optical imaging window between 900–1,700 nm, where tissue scattering is extremely low [96]. The implementation of NIR-II fluorescence may therefore revolutionize fluorescence imaging by improving depth penetration, spatial and temporal resolution, and the SBR [97]. Until new advances are made with NIR-II imaging, the development of NIR-I contrast agents and their approval by the FDA are the rate-limiting step in the clinical utilization of intraoperative fluorescence technology.

Aside from fluorescence imaging systems, extensive efforts are being made to integrate current medical imaging modalities in robust surgery rooms for intraoperative surgical navigation. The concepts of the Advanced Multimodal Image-Guided Operating Suite (AMIGO) and the guided therapeutics operation room (GTx OR) have transformed preprocedural and intraprocedural imaging during surgery by providing clinical, translational research facilities with various imaging modalities [98]. AMIGO enables precise identification, targeted biopsy, and complete resection of tumors, which are procedures that can be transferred to dedicated molecular image-guided therapy suites for MRI and PET/CT. The GTx OR utilizes a dual-source and dual-energy CT scanner, robotic cone-beam CT/fluoroscopy, X-ray imaging, an electromagnetic navigation system, and an NIR fluorescence system within the same operating room to develop real-time 3D therapy [98]. Having this complete array of advanced imaging and interventional surgical systems allows collaborating specialists to efficiently treat patients before, during, and after surgery without ever leaving the operating room [99]. Ultimately, the combination of AMIGO and intraoperative fluorescence imaging modalities, coupled with the development of NIR contrast agents, will optimize thoracic surgery in the future, reducing rates of remission and improving patient outcomes.

Conflict of interest

No potential conflict of interest relevant to this article was reported.

Acknowledgments

This study was supported by the US NIH grant NIBIB #R01-EB022230 and NCI #R21-CA223270. The contents of this paper are solely the responsibility of the authors and do not necessarily reflect the official views of the National Institutes of Health.

ORCID

Priyanka Das: https://orcid.org/0000-0001-5289-4550
Sheena Santos: https://orcid.org/0000-0002-6735-0334
G. Kate Park: https://orcid.org/0000-0003-4476-9084
Hoseok I: https://orcid.org/0000-0001-8930-8148
Hak Soo Choi: https://orcid.org/0000-0002-7982-6483

References

1. Park GK, Hoseok I, Kim GS, Hwang NS, Choi HS. *Optical spectroscopic imaging for cell therapy and tissue engineering*. Appl Spectrosc Rev 2018;53:360-75.
2. Owens EA, Henary M, El Fakhri G, Choi HS. *Tissue-specific near-infrared fluorescence imaging*. Acc Chem Res 2016; 49:1731-40.
3. Haidekker MA. *Computed tomography*. In: Haidekker MA, editor. *Medical imaging technology*. New York (NY): Springer; 2013. p. 37-53.
4. Osaki Y, Hatazawa J. *PET/SPECT*. Equil Res 2009;68:54-61.
5. Haidekker MA. *Magnetic resonance imaging*. In: Haidekker MA, editor. *Medical imaging technology*. New York (NY): Springer; 2013. p. 67-96.
6. Hu S, Kang H, Baek Y, El Fakhri G, Kuang A, Choi HS. *Real-time imaging of brain tumor for image-guided surgery*. Adv Healthc Mater 2018;7:1800066.
7. Haidekker MA. *X-ray projection imaging*. In: Haidekker MA, editor. *Medical imaging technology*. New York (NY): Springer; 2013. p. 13-35.
8. Haidekker MA. *Ultrasound imaging*. In: Haidekker MA, editor. *Medical imaging technology*. New York (NY): Springer; 2013. p. 97-110.
9. Owens EA, Lee S, Choi J, Henary M, Choi HS. *NIR fluorescent small molecules for intraoperative imaging*. Wiley Interdiscip Rev Nanomed Nanobiotechnol 2015;7:828-38.
10. Kim T, O'Brien C, Choi HS, Jeong MY. *Fluorescence molecular imaging systems for intraoperative image-guided surgery*. Appl Spectrosc Rev 2018;53:349-59.
11. Son J, Yi G, Yoo J, Park C, Koo H, Choi HS. *Light-responsive nanomedicine for biophotonic imaging and targeted therapy*. Adv Drug Deliv Rev 2019;138:133-47.
12. DSouza AV, Lin H, Henderson ER, Samkoe KS, Pogue BW. *Review of fluorescence guided surgery systems: identification of key performance capabilities beyond indocyanine green imaging*. J Biomed Opt 2016;21:80901.
13. Yang AW, Cho SU, Jeong MY, Choi HS. *NIR fluorescence imaging systems with optical packaging technology*. J Microelectron Packag Soc 2014;21:25-31.
14. Troyan SL, Kianzad V, Gibbs-Strauss SL, et al. *The FLARE intraoperative near-infrared fluorescence imaging system: a first-in-human clinical trial in breast cancer sentinel lymph node mapping*. Ann Surg Oncol 2009;16:2943-52.
15. Gioux S, Choi HS, Frangioni JV. *Image-guided surgery using invisible near-infrared light: fundamentals of clinical translation*. Mol Imaging 2010;9:237-55.
16. Choi HS, Gibbs SL, Lee JH, et al. *Targeted zwitterionic near-infrared fluorophores for improved optical imaging*. Nat Biotechnol 2013;31:148-53.
17. Hyun H, Henary M, Gao T, et al. *700-nm zwitterionic near-infrared fluorophores for dual-channel image-guided surgery*. Mol Imaging Biol 2016;18:52-61.
18. Ashitate Y, Kim SH, Tanaka E, et al. *Two-wavelength near-infrared fluorescence for the quantitation of drug antiplatelet effects in large animal model systems*. J Vasc Surg 2012;56:171-80.
19. Ashitate Y, Levitz A, Park MH, et al. *Endocrine-specific NIR fluorophores for adrenal gland targeting*. Chem Commun (Camb) 2016;52:10305-8.
20. Ashitate Y, Stockdale A, Choi HS, Laurence RG, Frangioni JV. *Real-time simultaneous near-infrared fluorescence imaging of bile duct and arterial anatomy*. J Surg Res 2012;176:7-13.
21. Ashitate Y, Vooght CS, Hutteman M, Oketokoun R, Choi HS, Frangioni JV. *Simultaneous assessment of luminal integrity and vascular perfusion of the gastrointestinal tract using dual-channel near-infrared fluorescence*. Mol Imaging 2012;11:301-8.
22. Hyun H, Owens EA, Wada H, et al. *Cartilage-specific near-infrared fluorophores for biomedical imaging*. Angew Chem Int Ed Engl 2015;54:8648-52.
23. Hyun H, Wada H, Bao K, et al. *Phosphonated near-infrared fluorophores for biomedical imaging of bone*. Angew Chem Int Ed Engl 2014;53:10668-72.
24. Hyun H, Park MH, Owens EA, et al. *Structure-inherent targeting of near-infrared fluorophores for parathyroid and thyroid gland imaging*. Nat Med 2015;21:192-7.
25. Kim SH, Lee JH, Hyun H, et al. *Near-infrared fluorescence imaging for noninvasive trafficking of scaffold degradation*. Sci Rep 2013;3:1198.
26. Owens EA, Hyun H, Dost TL, et al. *Near-infrared illumination of native tissues for image-guided surgery*. J Med Chem 2016;59:5311-23.
27. Owens EA, Hyun H, Kim SH, et al. *Highly charged cyanine fluorophores for trafficking scaffold degradation*. Biomed Mater 2013;8:014109.
28. Owens EA, Hyun H, Tawney JG, Choi HS, Henary M. *Correlating molecular character of NIR imaging agents with tissue-specific uptake*. J Med Chem 2015;58:4348-56.
29. Wada H, Hyun H, Kang H, et al. *Intraoperative near-infrared fluorescence imaging of thymus in preclinical models*. Ann Thorac Surg 2017;103:1132-41.
30. Wada H, Hyun H, Vargas C, et al. *Sentinel lymph node mapping of liver*. Ann Surg Oncol 2015;22 Suppl 3:S1147-55.
31. Ashitate Y, Hyun H, Kim SH, et al. *Simultaneous mapping of pan and sentinel lymph nodes for real-time image-guided surgery*. Theranostics 2014;4:693-700.
32. Wada H, Hyun H, Bao K, et al. *Multivalent mannose-decorated NIR nanoprobes for targeting pan lymph nodes*. Chem Eng J 2018;340:51-7.

33. Kajiwara N, Maeda J, Yoshida K, et al. *Maximizing use of robot-arm no. 3 in daVinci-assisted thoracic surgery*. Int Surg 2015;100:930-3.
34. Luo X, Mori K, Peters TM. *Advanced endoscopic navigation: surgical big data, methodology, and applications*. Annu Rev Biomed Eng 2018;20:221-51.
35. Han KN, Kim HK. *Imaging techniques for minimally invasive thoracic surgery-Korea University Guro Hospital experiences*. J Thorac Dis 2018;10(Suppl 6):S731-8.
36. Kumar A, Asaf BB. *Robotic thoracic surgery: the state of the art*. J Minim Access Surg 2015;11:60-7.
37. Palep JH. *Robotic assisted minimally invasive surgery*. J Minim Access Surg 2009;5:1-7.
38. Wagner OJ, Louie BE, Vallieres E, Aye RW, Farivar AS. *Near-infrared fluorescence imaging can help identify the contralateral phrenic nerve during robotic thymectomy*. Ann Thorac Surg 2012;94:622-5.
39. Latif MJ, Park BJ. *Robotics in general thoracic surgery procedures*. J Vis Surg 2017;3:44.
40. Suda T. *Transition from video-assisted thoracic surgery to robotic pulmonary surgery*. J Vis Surg 2017;3:55.
41. Veronesi G, Novellis P, Voulaz E, Alloisio M. *Robot-assisted surgery for lung cancer: state of the art and perspectives*. Lung Cancer 2016;101:28-34.
42. Drevet G, Conti M, Deslauriers J. *Surgical anatomy of the tracheobronchial tree*. J Thorac Dis 2016;8(Suppl 2):S121-9.
43. Miot-Noirault E, Guicheux J, Vidal A, et al. *In vivo experimental imaging of osteochondral defects and their healing using (99m)Tc-NTP 15-5 radiotracer*. Eur J Nucl Med Mol Imaging 2012;39:1169-72.
44. Jo D, Hyun H. *Structure-inherent targeting of near-infrared fluorophores for image-guided surgery*. Chonnam Med J 2017;53:95-102.
45. Mailis A, Umana M, Feindel CM. *Anterior intercostal nerve damage after coronary artery bypass graft surgery with use of internal thoracic artery graft*. Ann Thorac Surg 2000;69:1455-8.
46. Kretschmer T, Heinen CW, Antoniadis G, Richter HP, Konig RW. *Iatrogenic nerve injuries*. Neurosurg Clin N Am 2009;20:73-90.
47. Katahira A, Niikura H, Kaiho Y, et al. *Intraoperative electrical stimulation of the pelvic splanchnic nerves during nerve-sparing radical hysterectomy*. Gynecol Oncol 2005;98:462-6.
48. Cotero VE, Siclovan T, Zhang R, et al. *Intraoperative fluorescence imaging of peripheral and central nerves through a myelin-selective contrast agent*. Mol Imaging Biol 2012;14:708-17.
49. Vinegoni C, Botnaru I, Aikawa E, et al. *Indocyanine green enables near-infrared fluorescence imaging of lipid-rich, inflamed atherosclerotic plaques*. Sci Transl Med 2011;3:-84ra45.
50. Shimada Y, Okumura T, Nagata T, et al. *Usefulness of blood supply visualization by indocyanine green fluorescence for reconstruction during esophagectomy*. Esophagus 2011;8:259-66.
51. Ly HQ, Hoshino K, Pomerantseva I, et al. *In vivo myocardial distribution of multipotent progenitor cells following intracoronary delivery in a swine model of myocardial infarction*. Eur Heart J 2009;30:2861-8.
52. Pajouhesh H, Lenz GR. *Medicinal chemical properties of successful central nervous system drugs*. NeuroRx 2005;2: 541-53.
53. He K, Zhou J, Yang F, et al. *Near-infrared intraoperative imaging of thoracic sympathetic nerves: from preclinical study to clinical trial*. Theranostics 2018;8:304-13.
54. Gibbs-Strauss SL, Nasr KA, Fish KM, et al. *Nerve-highlighting fluorescent contrast agents for image-guided surgery*. Mol Imaging 2011;10:91-101.
55. Hingorani DV, Whitney MA, Friedman B, et al. *Nerve-targeted probes for fluorescence-guided intraoperative imaging*. Theranostics 2018;8:4226-37.
56. Park MH, Hyun H, Ashitate Y, et al. *Prototype nerve-specific near-infrared fluorophores*. Theranostics 2014;4:823-33.
57. Reagan-Shaw S, Nihal M, Ahmad N. *Dose translation from animal to human studies revisited*. FASEB J 2008;22: 659-61.
58. Araki T, Nishino M, Gao W, et al. *Normal thymus in adults: appearance on CT and associations with age, sex, BMI and smoking*. Eur Radiol 2016;26:15-24.
59. Nasseri F, Eftekhari F. *Clinical and radiologic review of the normal and abnormal thymus: pearls and pitfalls*. Radiographics 2010;30:413-28.
60. Chung JE, Tan S, Gao SJ, et al. *Self-assembled micellar nanocomplexes comprising green tea catechin derivatives and protein drugs for cancer therapy*. Nat Nanotechnol 2014;9:907-12.
61. Chang JM, Lee HJ, Goo JM, et al. *False positive and false negative FDG-PET scans in various thoracic diseases*. Korean J Radiol 2006;7:57-69.
62. Ofori LO, Withana NP, Prestwood TR, et al. *Design of protease activated optical contrast agents that exploit a latent lysosomotropic effect for use in fluorescence-guided surgery*. ACS Chem Biol 2015;10:1977-88.
63. Predina JD, Newton AD, Desphande C, Singhal S. *Near-infrared intraoperative imaging during resection of an anterior mediastinal soft tissue sarcoma*. Mol Clin Oncol 2018; 8:86-8.
64. Zhou J, Yang F, Jiang G, Wang J. *Applications of indocyanine green based near-infrared fluorescence imaging in thoracic surgery*. J Thorac Dis 2016;8(Suppl 9):S738-43.
65. Wen CT, Liu YY, Fang HY, Hsieh MJ, Chao YK. *Image-guided video-assisted thoracoscopic small lung tumor resection using near-infrared marking*. Surg Endosc 2018;32:4673-80.
66. Okusanya OT, Holt D, Heitjan D, et al. *Intraoperative near-infrared imaging can identify pulmonary nodules*. Ann Thorac Surg 2014;98:1223-30.
67. Hihara J, Mukaida H, Hirabayashi N. *Gastrointestinal stromal tumor of the esophagus: current issues of diagnosis,*

surgery and drug therapy. Transl Gastroenterol Hepatol 2018;3:6.
68. Fujimoto S, Muguruma N, Okamoto K, et al. *A novel theranostic combination of near-infrared fluorescence imaging and laser irradiation targeting c-KIT for gastrointestinal stromal tumors*. Theranostics 2018;8:2313-28.
69. Kang H, Gravier J, Bao K, et al. *Renal clearable organic nanocarriers for bioimaging and drug delivery*. Adv Mater 2016;28:8162-8.
70. Li X, Chen S, Jiang L, et al. *Precise intraoperative sentinel lymph node biopsies guided by lymphatic drainage in breast cancer*. Oncotarget 2017;8:63064-72.
71. Khullar O, Frangioni JV, Grinstaff M, Colson YL. *Image-guided sentinel lymph node mapping and nanotechnology-based nodal treatment in lung cancer using invisible near-infrared fluorescent light*. Semin Thorac Cardiovasc Surg 2009;21:309-15.
72. Khullar OV, Gilmore DM, Matsui A, Ashitate Y, Colson YL. *Preclinical study of near-infrared-guided sentinel lymph node mapping of the porcine lung*. Ann Thorac Surg 2013;95:312-8.
73. Soltesz EG, Kim S, Laurence RG, et al. *Intraoperative sentinel lymph node mapping of the lung using near-infrared fluorescent quantum dots*. Ann Thorac Surg 2005;79:269-77.
74. Kim S, Lim YT, Soltesz EG, et al. *Near-infrared fluorescent type II quantum dots for sentinel lymph node mapping*. Nat Biotechnol 2004;22:93-7.
75. Frangioni JV, Kim SW, Ohnishi S, Kim S, Bawendi MG. *Sentinel lymph node mapping with type-II quantum dots*. Methods Mol Biol 2007;374:147-59.
76. Parungo CP, Ohnishi S, De Grand AM, et al. *In vivo optical imaging of pleural space drainage to lymph nodes of prognostic significance*. Ann Surg Oncol 2004;11:1085-92.
77. Parungo CP, Colson YL, Kim SW, et al. *Sentinel lymph node mapping of the pleural space*. Chest 2005;127:1799-804.
78. Chi C, Ye J, Ding H, et al. *Use of indocyanine green for detecting the sentinel lymph node in breast cancer patients: from preclinical evaluation to clinical validation*. PLoS One 2013;8:e83927.
79. Sugie T, Kinoshita T, Masuda N, et al. *Evaluation of the clinical utility of the ICG fluorescence method compared with the radioisotope method for sentinel lymph node biopsy in breast cancer*. Ann Surg Oncol 2016;23:44-50.
80. Grischke EM, Rohm C, Hahn M, Helms G, Brucker S, Wallwiener D. *ICG fluorescence technique for the detection of sentinel lymph nodes in breast cancer: results of a prospective open-label clinical trial*. Geburtshilfe Frauenheilkd 2015;75:935-40.
81. Hirche C, Murawa D, Mohr Z, Kneif S, Hunerbein M. *ICG fluorescence-guided sentinel node biopsy for axillary nodal staging in breast cancer*. Breast Cancer Res Treat 2010; 121:373-8.
82. Tagaya N, Yamazaki R, Nakagawa A, et al. *Intraoperative identification of sentinel lymph nodes by near-infrared fluorescence imaging in patients with breast cancer*. Am J Surg 2008;195:850-3.
83. Guo J, Yang H, Wang S, et al. *Comparison of sentinel lymph node biopsy guided by indocyanine green, blue dye, and their combination in breast cancer patients: a prospective cohort study*. World J Surg Oncol 2017;15:196.
84. Tagaya N, Aoyagi H, Nakagawa A, et al. *A novel approach for sentinel lymph node identification using fluorescence imaging and image overlay navigation surgery in patients with breast cancer*. World J Surg 2011;35:154-8.
85. Van der Vorst JR, Schaafsma BE, Verbeek FP, et al. *Randomized comparison of near-infrared fluorescence imaging using indocyanine green and 99(m) technetium with or without patent blue for the sentinel lymph node procedure in breast cancer patients*. Ann Surg Oncol 2012;19:4104-11.
86. Schaafsma BE, Verbeek FP, Rietbergen DD, et al. *Clinical trial of combined radio- and fluorescence-guided sentinel lymph node biopsy in breast cancer*. Br J Surg 2013;100: 1037-44.
87. Tong M, Guo W, Gao W. *Use of fluorescence imaging in combination with patent blue dye versus patent blue dye alone in sentinel lymph node biopsy in breast cancer*. J Breast Cancer 2014;17:250-5.
88. Toh U, Iwakuma N, Mishima M, Okabe M, Nakagawa S, Akagi Y. *Navigation surgery for intraoperative sentinel lymph node detection using Indocyanine green (ICG) fluorescence real-time imaging in breast cancer*. Breast Cancer Res Treat 2015;153:337-44.
89. Liu J, Huang L, Wang N, Chen P. *Indocyanine green detects sentinel lymph nodes in early breast cancer*. J Int Med Res 2017;45:514-24.
90. Papathemelis T, Jablonski E, Scharl A, et al. *Sentinel lymph node biopsy in breast cancer patients by means of indocyanine green using the Karl Storz VITOM(R) fluorescence camera*. Biomed Res Int 2018;2018:6251468.
91. Yamamoto M, Sasaguri S, Sato T. *Assessing intraoperative blood flow in cardiovascular surgery*. Surg Today 2011;41: 1467-74.
92. Marshall MV, Rasmussen JC, Tan IC, et al. *Near-infrared fluorescence imaging in humans with indocyanine green: a review and update*. Open Surg Oncol J 2010;2:12-25.
93. Lin MW, Chen JS. *Image-guided techniques for localizing pulmonary nodules in thoracoscopic surgery*. J Thorac Dis 2016;8(Suppl 9):S749-55.
94. Owens SL. *Indocyanine green angiography*. Br J Ophthalmol 1996;80:263-6.
95. Hackethal A, Hirschburger M, Eicker SO, Mucke T, Lindner C, Buchweitz O. *Role of indocyanine green in fluorescence imaging with near-infrared light to identify sentinel lymph nodes, lymphatic vessels and pathways prior to surgery: a critical evaluation of options*. Geburtshilfe Frauenheilkd 2018;78:54-62.
96. Hong G, Lee JC, Robinson JT, et al. *Multifunctional in vivo vascular imaging using near-infrared II fluorescence*. Nat

Med 2012;18:1841-6.
97. Haque A, Faizi MS, Rather JA, Khan MS. *Next generation NIR fluorophores for tumor imaging and fluorescence-guided surgery: a review*. Bioorg Med Chem 2017;25: 2017-34.
98. Ujiie H, Effat A, Yasufuku K. *Image-guided thoracic surgery in the hybrid operation room.* J Vis Surg 2017;3:148.
99. Tempany CM, Jayender J, Kapur T, et al. *Multimodal imaging for improved diagnosis and treatment of cancers.* Cancer 2015;121:817-27.